Ecotoxicology and Environmental Safety 241 (2022) 113779

Contents lists available at ScienceDirect

Ecotoxicology and Environmental Safety

journal homepage: www.elsevier.com/locate/ecoenv

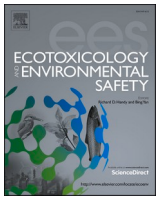

Valproic acid counteracts polycyclic aromatic hydrocarbons (PAHs)-induced tumorigenic effects by regulating the polarization of macrophages

Yisha Zhang [a], David Lim [b,c], Zuchao Cai [a], Junxuan Peng [a], Beidi Jia [a], Guoliang Chu [a], Fengmei Zhang [a], Chao Dong [a,*], Zhihui Feng [a,*]

[a] Department of Occupational Health and Occupational Medicine, School of Public Health, Cheeloo College of Medicine, Shandong University, Jinan 250012, Shandong, China
[b] Translational Health Research Institute, School of Health Sciences, Western Sydney University, Campbelltown, New South Wales, Australia
[c] College of Medicine and Public Health, Flinders University, Bedford Park, South Australia, Australia

ARTICLE INFO

Edited by Professor Bing Yan

Keywords:
PAHs
VPA
Macrophages
Vasculature

ABSTRACT

Polycyclic aromatic hydrocarbons (PAHs) are common persistent organic pollutants that are carcinogenic, teratogenic and mutagenic, causing a variety of harm to human health. In this study, we investigated the mechanism of how valproic acid (VPA) interferes with the carcinogenesis of PAHs protect normal tissues *via* the regulation of macrophages' function. Using the established model of transformed malignant breast cancer by 7,12-dimethylbenz[*a*]anthracene (DMBA), a representative PAH carcinogen, we discovered VPA induces the polarization of macrophages toward the M1 phenotype in the tumor tissues, facilitates the expression of pro-inflammatory cytokines such as IFN-γ, IL-12 and TNF-α, activates $CD8^+$ T cells to secret Granzyme B thus to promote the apoptosis of tumor cells and suppresses the viability of vascular endothelial cells in tissue stroma of tumor. Surprisingly, VPA selectively induces macrophages to polarize towards the M2 phenotype in normal tissues and promotes the expression of anti-inflammatory cytokines such as IL-10 to enhance cell proliferation. Additionally, at the cellular level, VPA can directly regulate the polarization of macrophages to affect the growth of vascular endothelial cells by simulating the living conditions of tumor and normal cells. Collectively, VPA exerts an interventional effect on tumor growth and a protective effect on normal tissues by regulation of selective macrophages' polarization in their microenvironment.

1. Introduction

Polycyclic aromatic hydrocarbons (PAHs) are a type of persistent organic pollutants and mainly derive from anthropogenic activities, such as the incomplete combustion or high-temperature pyrolysis of various fuels and biomass, vehicle emissions and oil spills (Bezza and Chirwa, 2016; Sun et al., 2021). PAHs are widely distributed throughout the environment in the air, water, sediment and soil (Shi et al., 2015). PAHs are carcinogenic, teratogenic and mutagenic, and cause a variety of harm to human health (Bezza and Chirwa, 2016; Kim et al., 2013; Yang et al., 2008). 7, 12-Dimethylbenzanthracene (DMBA) is a representative compound of PAHs and the most common carcinogen used for inducing breast cancer in animals (Manjanatha et al., 1996). Previously, we have successfully induced primary breast tumors in female Sprague Dawley (SD) rats with DMBA (Wang et al., 2014b).

Valproic acid (VPA), a histone deacetylase inhibitor (HDACi), has previously been shown to have epigenetic properties by interfering with histone deacetylation, histone remodeling, and the methylation status of DNA and histones (Gu et al., 2012; Mello, 2021; Milutinovic et al., 2007; Vidal and Mello, 2020), thus altering the expression of transcription

Abbreviations: PAHs, polycyclic aromatic hydrocarbons; VPA, valproic acid; HDACi, histone deacetylase inhibitor; DMBA, 7,12-dimethylbenz[*a*]anthracene; SD, Sprague-Dawley; TAMs, tumor-associated macrophages; HUVEC, human umbilical vein endothelial cells; BrdU, 5-Bromo-2′-deoxyuridine; HE, hematoxylin and eosin; IHC, immunohistochemistry; HPTA, 2-hexyl-4-pentynoic acid.

* Correspondence to: Department of Occupational Health and Occupational Medicine, School of Public Health, Cheeloo College of Medicine, Shandong University, 44 Wenhua Xi Road, Jinan 250012, Shandong, China.
E-mail addresses: chaodong@sdu.edu.cn (C. Dong), fengzhihui@sdu.edu.cn (Z. Feng).

https://doi.org/10.1016/j.ecoenv.2022.113779
Received 20 February 2022; Received in revised form 31 May 2022; Accepted 14 June 2022
Available online 22 June 2022

factors leading to modulation of gene expression, resulting in reduced tumor proliferation, increased cell differentiation and apoptosis (Sharma et al., 2013; Wagner et al., 2010). Furthermore, we and others have demonstrated that VPA as a neoadjunctive and adjunctive therapeutic agent in breast cancer, VPA disrupts the RPA2-p-mediated DNA repair pathway to enhance the cytotoxic effects of radiotherapy and chemotherapy (Su et al., 2021). Whilst VPA is not yet approved by the US Food and Drug Administration and European Medicines Agency for oncological treatment, VPA has been approved and safely used in the treatment of epilepsy and manic episodes in bipolar disorders (Watanabe et al., 2017). In DMBA-induced rat models, VPA was previously shown to delay tumor formation, reduce tumor occurrence rate, attenuate tumor growth, and exert a protective effect on normal tissues when VPA was administrated for the intervention at the concentrations of 50 mg/kg and 100 mg/kg, the discovery in addition to VPA epigenetic properties is its potential immunoregulatory functions in the tumor microenvironment (Peng et al., 2020). Although VPA has been shown to recruit macrophages to tumor sites, the underlying mechanism remains elusive (Su et al., 2021).

Macrophages exist within many tissues and mediate important biological functions including host defense against pathogens, removal of cellular debris and wound repair (Gordon and Martinez, 2010). Within tissues, macrophages have strong plasticity (Obeid et al., 2013) and their polarization status is directed by signals received from their surrounding microenvironment (Epelman et al., 2014). Macrophages can be polarized into two distinct phenotypes: the classical activated or the alternative activated macrophages (Long et al., 2019; Reddy et al., 2018). Macrophages can be polarized either into M1-like macrophages with IFN-γ and lipopolysaccharide (LPS) (their surface marker is CD86 (Wang et al., 2019)), or into M2-like macrophages with IL-4, IL-10 and IL-13 (their surface marker is CD163) (Martinez and Gordon, 2014; Tang, 2013). M1 macrophage markers, such as CD86, TNF-α, inducible nitric oxide synthase (iNOS), and IL-12, possess strong antigen-presenting ability and phagocytosis (Kim et al., 2018). For instance, TNF-α can mediate the presentation of tumor antigens by macrophages, activate cellular immune responses, and kill tumor cells (Zhang et al., 2012). iNOS can produce nitric oxide (NO) to kill tumor cells and achieve anti-tumor activity (Arlauckas et al., 2017; Ring et al., 2018). In addition, M1 macrophages are critical for the effective control of bacterial infections (Qian and Pollard, 2010). M2 macrophage markers include CD163, Arginase-1 (Arg-1), IL-10 and TGF-β (Tao et al., 2020). Arg-1, a functional marker of M2 macrophage, promotes the proliferation and growth of tumor cells (Xu and Wang, 2011). IL-10 can inhibit the production of pro-inflammatory factors and induce macrophages to polarize to the M2 phenotype, which promotes angiogenesis and tumor cell growth (Qiu et al., 2018).

Tumor-associated macrophages (TAMs) exist ubiquitously in the tumor tissues. The TAMs are similar to the M2-polarized phenotype and usually associated with tumor growth, metastasis and angiogenesis (Long et al., 2019; Morrison, 2016; Roma-Rodrigues et al., 2019). Since TAMs are the most influential for tumor progression and their increased presence within tumors is usually tightly associated with poorer prognosis (Obeid et al., 2013; Qiu et al., 2018), and lower overall survival rates (DeNardo et al., 2011), TAMs have emerged as a major obstacle for cancer immunotherapy (Ino et al., 2013; Medrek et al., 2012; Obeid et al., 2013; Qian and Pollard, 2010). The repolarization of macrophages may be crucial in the development of novel cancer therapy.

Studies have shown that VPA can influence the phenotype and function of macrophages, and plays an important role in immune regulation and inflammation (Ji et al., 2013; Song et al., 2015). In breast cancer tissues, a different HDACi, TMP195 was shown to induce the recruitment and differentiation of high phagocytosis and irritant macrophages (Guerriero et al., 2017). Similarly, low doses of another HDACi, trichostatin-A (TSA) was shown to reshape the tumor microenvironment by regulating the activity of infiltrating macrophages; and in combination with anti-PD-L1, significantly inhibited tumor growth (Li et al., 2021). Accumulating studies support the proposition to further investigate the potential application of VPA in low-cost immunotherapy in cancer treatment.

Whilst we have previously reported that intervention with VPA in a DMBA-induced primary rat model of breast cancer exerts bidirectional regulatory effects, it remains unclear whether VPA-mediated the inhibition of tumor tissues and the protection of normal tissues are through the regulation of macrophage-mediated immune response (Peng et al., 2020). We hypothesized that VPA could activate immune pathways to inhibit tumors and protect normal tissues exerting bidirectional effects. In this study, we found that VPA could induce the polarization of macrophages toward the M1 phenotype in the DMBA-induced model of breast cancer tissues, and polarization toward the M2 phenotype in normal tissues to achieve anti-inflammatory effects which were also validated vascular endothelial cells, illuminating the underlying mechanism of VPA-mediated bidirectional effects, at least in part, depends on immune response.

2. Methods and materials

2.1. The establishment of the animal model

Female SD rats were purchased from Peng Yue Laboratory Animal Co. Ltd., Jinan, China. The experiments were performed in concordance with the requirements of the Shandong University Human and Animal Ethics Research Committee (project identification code 81472800, ethics approved 3 March 2014). The rats were randomly divided into six groups: untreated control group, VPA (P4543, Sigma) 50 mg/kg group, VPA 100 mg/kg group, DMBA (D3254, Sigma) group, DMBA+VPA 50 mg/kg group and DMBA+VPA 100 mg/kg group.

Regarding the selection of the VPA dose, our group selected 200 mg/kg equivalent to clinical treatment of epilepsy in the animal experiments for tumor treatment research (Liu et al., 2021). In this study, the dose of VPA (50 mg/kg and 100 mg/kg) lower than the therapeutic dose was selected to prevent the occurrence and development of tumors. The establishment of the animal model is reported in our previous article (Peng et al., 2020). At the same time, according to the animal experimental doses of 50 and 100 mg/kg, the VPA doses used at the cellular level were calculated to be 0.2 and 0.4 mM (Liu et al., 2021).

2.2. Cell culture

Human umbilical vein endothelial cells (HUVEC) and RAW264.7 cells were purchased from American Type Culture Collection (ATCC) and cultured in DMEM (CM10017, Macgene) medium with 10% Fetal Bovine Serum (10270106, Gibco) and 1% Penicillin-Streptomycin (V900929, Sigma). MCF10A and DMBA-transformed MCF10A (MCF10A-DMBA, established by our group (Liu et al., 2021)) cells were maintained in DMEM/F12 (CM10092, Macgene) supplemented with 5% Horse Serum (26050070 , Gibco), 0.1% Insulin (10320000, Sigma), 0.1% Cholera toxin (CC104, Macgene), 0.05% Hydrocortisone (CC103, Macgene), 0.02% EGF (E5036, Sigma) and 1% Penicillin-Streptomycin (V900929, Sigma). All cells were validated to be mycoplasma-free, and maintained at 37 °C in 5% CO_2.

2.3. Western blot analysis

The protein samples from all groups were homogenized in RIPA buffer with protease inhibitors (Cocktail, HJ200916, Servicebio) and clarified by centrifugation, proteins were quantified by BCA method. The protocol is as follow: SDS-PAGE gel making, sample loading, electrophoresis, transferring to PVDF membranes, milk blocking, the incubation with primary and secondary antibodies, and chemiluminescence. The primary antibodies used: Cleaved caspase-3 (1:1000, Asp175, CST), Granzyme B (1:500, sc-8022, Santa Cruz), β-actin (1:2000, TA-09, Zsgb-Bio). The secondary antibodies were goat anti-mouse lgG (H + L)

(1:5000, 31430, Thermo Fisher) and goat anti-rabbit lgG (H + L) (1:5000, 31460, Thermo Fisher). The relative protein intensities were quantified by ImageJ software.

2.4. BrdU incorporation and HE staining

5-Bromo-2′ -deoxyuridine (BrdU) (B5002, Sigma) was injected intraperitoneally at a dose of 100 mg/kg 24 h prior to tissue harvest. Non-tumor tissues were fixed in 4% paraformaldehyde solution overnight, embedded in paraffin and serially sectioned 5 μm thick for hematoxylin and eosin (HE) staining following the manufacture's procedure guidelines.

2.5. Immunohistochemistry (IHC)

The tissue sections were deparaffinized with xylene, hydrated with 100–75% ethanol and washed with distilled water for 5 min, then boiled in sodium citrate solution at > 92 °C for 20 min for antigen retrieval. The sections were then cooled down to room temperature for 30 min and washed with distilled water three times. For BrdU staining, the sections were immersed in 1 M hydrochloric acid for 1 h and then neutralized with 0.1 M sodium borate buffer for 10 min, washed with TBS three times. Subsequently, the sections were incubated in 3% hydrogen peroxide for 15 min to remove endogenous peroxidase and washed again with TBS, before incubation with 10% goat serum in 1% BSA for 1 h at room temperature to block nonspecific bindings. The sections were then incubated at 4 °C in hydration chambers overnight with primary and secondary antibodies. The primary antibodies used: BrdU (1:50, Cat.347580, BD), Cleaved Caspase-3 (1:200, Asp175, CST), F4/80 (1:300, 123102, Biolegend), CD68 (1:800, GB11067, Servicebio), CD11b (1:5000, ab133357, Abcam), CD8 (1:500, GB11068, Servicebio), and Granzyme B (1:200, sc-8022, Santa Cruz). Secondary antibodies used in this study: biotinylated goat anti-rabbit IgG (1:300, BA-1000, Vector), biotinylated goat anti-mouse IgG (1:300, BA-9200, Vector), biotinylated goat anti-rat IgG (1:300, BA-9400, Vector). Images were captured by digital biological microscope (NLCD-500). The relative number of positive cells was further quantified by Image Pro Plus software (Media Cybrenetics).

2.6. Immunofluorescence

The procedure for immunofluorescence is the same as the procedure for immunohistochemistry prior to incubation of the primary antibody, except that the immunofluorescence procedure after the incubation of the secondary antibody is in the dark. The primary antibodies included CD31 (1:200, GB12063, Servicebio), F4/80 (1:200, 123101, BioLegend), CD11b (1:2000, ab133357, Abcam), EpCAM (1:200, sc-66020, Santa Cruz), CD8 (1:500, GB11068, Servicebio), and Granzyme B (1:200, sc-8022, Santa Cruz). Secondary antibodies were Alexa Fluor® 488 chicken anti-rabbit IgG(H+L) (1:300; A21441, Molecular probes), Alexa Fluor® 488 goat anti-mouse IgG (H+L) (1:300; A11029, Molecular probes), Alexa Fluor® 594 goat anti-mouse IgG (H+L) (1:300; A11032, Molecular probes), Alexa Fluor® 594 chicken anti-rat IgG (H+L) (1:300; A21417, Molecular probes). Images were captured using Fluorescence Microscope (OLYMPUS BX53).

2.6.1. RNA isolation and Real-time quantitative reverse transcriptase PCR (RT-qPCR)

After harvesting the rat tissues, the samples were snap-freeze in liquid nitrogen and stored at − 80 °C for RT-qPCR analysis. The RNA in animal tissues and cells was isolated by FastPure Cell/Tissue Total RNA Isolation Kit (Vazyme) and the concentration of RNA was quantified by NanoDrop ND-2000 spectrophotometer (Nadro Drop Technologies, Wilmington, DE, USA). Complementary DNA (cDNA) synthesis was performed using the RevertAid First Strand cDNA Synthesis Kit (Thermo). The real-time PCR was performed with the indicated primers, cDNA and Maxima SYBR Green (Thermo) on Light Cycler® 480II (Roche Applied Science, Indianapolis, IN, USA).

The C_t values (threshold cycle number) were acquired by the Light Cycler® 480 Software release 1.5.0 SP4 software and analyzed using $2^{-\Delta\Delta CT}$ method. $\triangle\triangle C_t$ = experimental group $\triangle C_t$ - control group $\triangle C_t$, $\triangle C_t$ = (average C_t of the target gene of the control sample - average Ct of the control sample GAPDH). Primer sequences used in the study are listed in Table 1.

2.7. MTT assay

MCF10A and MCF10A-DMBA cells were seeded in P60 dishes, the culture medium was changed after cell attaching. After 24 h, the culture was centrifuged to collect the medium supernatant, which was subsequently added to the P35 dishes at a 1:1 (conditioned medium: macrophage fresh medium) medium volume ratio seeded with RAW264.7 cells. The RAW264.7 cells were treated with 0.2 mM VPA or 0.4 mM VPA for 24 h, after which the cells were lysed by repeated freeze-thawing in PBS, and lysates were collected. HUVEC cells were seeded in the 96-well plates and cultured with MCF10A and MCF10A-DMBA cells conditioned medium for 24 h. Lysates were then extracted and added to HUVEC cells at a 2:3 (macrophage lysates and HUVEC cell culture medium) medium volume ratio. Following treatments, MTT solution (5 mg/ml, Sigma, M2128) was added to the treated cells and incubated for 4 h at 37 °C. After which, 120 ml dimethyl sulfoxide was added to each well. The absorbance of the solution was measured using an enzyme-labeled instrument (Tecan, Infinite M200 Pro) at 490 nm and

Table 1
The primer sequences used in this study.

Oligo Name (Rat)	Primer Sequence (5′−3′)
GAPDH	Forward: AGT GCC AGC CTC GTC TCA TA
	Reverse: GAT GGT GAT GGG TTT CCC GT
CD86	Forward: AAG CCC GTG TCC TTG ATC TG
	Reverse: AGA CAT GTG TAA CCT GCA CCA T
TNF-α	Forward: ATG GGC TCC CTC TCA TCA GTT CC
	Reverse: GCT CCT CCG CTT GGT GGT TTG
IFN-γ	Forward: ACA ACC CAC AGA TCC AGC ACA AAG
	Reverse: CAC CGA CTC CTT TTC CGC TTC C
IL-12	Forward: CCT CAA GTT CTT CGT CCG CAT CC
	Reverse: CAT TGG ACT TCG GCA GAG GTC TTC
iNOS	Forward: GAG ACG CAC AGG CAG AGG TTG
	Reverse: AGC AGG CAC ACG CAA TGA TGG
MHC-II	Forward: TGT GGT TGT GCT GAT GGT GCT G
	Reverse: GCT GCG TCC CGT TGG TGT AG
CD163	Forward: AGC ATG GCA CAG GTC ATT CA
	Reverse: GGT CAC AAA ACT TCA ACC GGA
TGF-β	Forward: GAC CGC AAC AAC GCA ATC TAT GAC
	Reverse: CTG GCA CTG CTT CCC GAA TGT C
IL-4	Forward: CAA GGA ACA CCA CGG AGA ACG AG
	Reverse: CTT CAA GCA CGG AGG TAC ATC ACG
IL-10	Forward: CTG CTC TTA CTG GCT GGA GTG AAG
	Reverse: TGG GTC TGG CTG ACT GGG AAG
Arg-1	Forward: TGG ACC CTG GGG AAC ACT AT
	Reverse: GTA GCC GGG GTG AAT ACT GG
Oligo Name (Mouse)	Primer Sequence (5′−3′)
GAPDH	Forward: GGT TGT CTC CTG CGA CTT CA
	Reverse: GGT GGT CCA GGG TTT CTT ACT C
CD86	Forward: ACG GAG TCA ATG AAG ATT TCC T
	Reverse: GAT TCG GCT TCT TGT GAC ATA C
TNF-α	Forward: ATG TCT CAG CCT CTT CTC ATT C
	Reverse: GCT CCT CCG CTT GGT GGT TTG
IFN-γ	Forward: CTT GAA AGA CAA TCA GGC CAT C
	Reverse: CTT GGC AAT ACT CAT GAA TGC A
IL-12	Forward: TGA GAA GTA TTC AGT GTC CTG C
	Reverse: CTG TGA GTT CTT CAA AGG CTT C
CD163	Forward: GTT TGT GGA GCC ATT CTA TTG G
	Reverse: GGA AAC TGT AAG TCG CTG AAT C
TGF-β	Forward: CCA GAT CCT GTC CAA ACT AAG G
	Reverse: CTC TTT AGC ATA GTA GTC CGC T
IL-10	Forward: TTC TTT CAA ACA AAG GAC CAG C
	Reverse: GCA ACC CAA GTA ACC CTT AAA G

532 nm.

2.8. ELISA

MCF10A and MCF10A-DMBA cells were seeded in P60 dishes, the culture medium was changed after cell attaching. After 24 h, the culture was centrifuged to collect the medium supernatant, which was subsequently added to the P35 dishes at a 1:1 (conditioned medium: macrophage fresh medium) medium volume ratio seeded with RAW264.7 cells. The RAW264.7 cells were treated with 0.2 mM or 0.4 mM VPA for 24 h, after which the cells were lysed by repeated freeze-thawing in PBS, lysates were collected. Cytokines detection (IL-12, IL-10) were performed using ELISA kits (1211232, 1211002, DAKEWE, China).

2.9. Statistical analysis

All statistical analyses were performed using Student's *t*-test on SPSS, Version 25.0 (Armonk, NY: IBM Corp; licensed to Shandong University). The data are expressed as mean ± standard deviation (SD). The *P* values were designated as: *, $P < 0.05$; **, $P < 0.01$, indicating a statistically significant difference.

3. Results

3.1. VPA intervenes tumor growth and activates the macrophages within breast tumors

We have previously reported that VPA intervenes the environmental carcinogen DMBA-induced primary breast cancer in rats and the intervention schedule of VPA was shown (Fig. 1A). By HE staining, we found few mammary ducts and a large amount of loose connective tissue was observed in normal breast tissues, there was no noticeable difference in the VPA-only treated groups compared with the control (Fig. 1B). By comparison, malignant cells, pathological dysplasia and interstitial fibrosis were observed in the DMBA-treated groups (Fig. 1B). In the DMBA-induced tumors treated with VPA (50 mg/kg or 100 mg/kg), there were more vacuoles structures and necrotic cells, thus suggesting that VPA intervenes tumor growth induced by DMBA.

The IHC and Western blotting experiments were further performed using the apoptosis-related protein, cleaved caspase-3. In the normal breast tissue, no remarkable differences between the VPA-only and control groups were observed ($P > 0.05$). While in the DMBA groups, cleaved caspase-3 was significantly increased after VPA (50 mg/kg or 100 mg/kg) intervention as assessed by IHC (Fig. 1C left, $P < 0.01$) and Western blotting (Fig. 1C right, $P < 0.01$), thus suggesting that VPA promoted the apoptosis of DMBA-induced breast tumor cells. We also performed immunofluorescence staining with the vascular endothelial

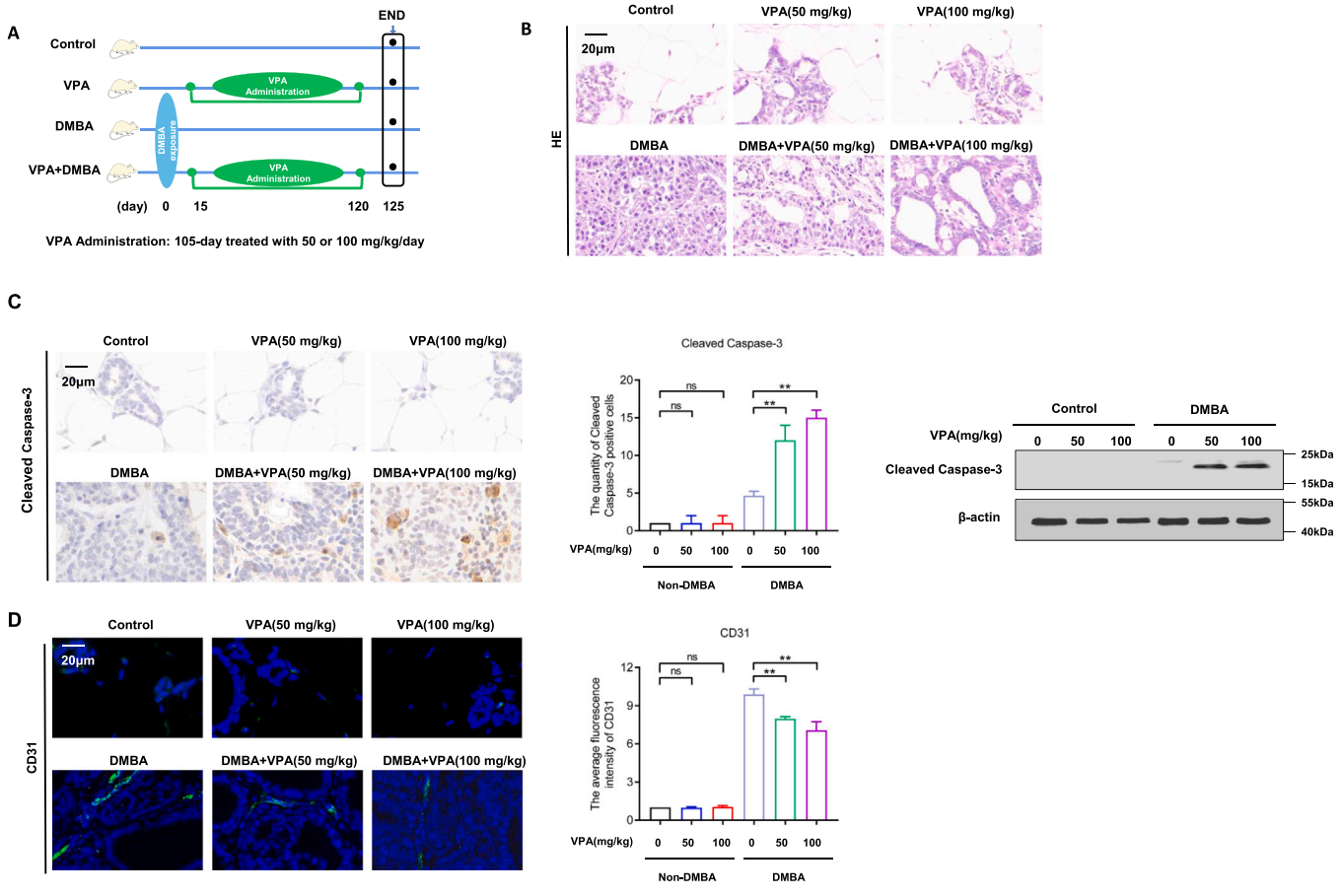

Fig. 1. VPA intervenes tumor growth in DMBA-induced breast cancer in rat. (A) The schematic diagram of DMBA-induced breast cancer in our rat model and VPA administration. 50 mg/kg/day and 100 mg/kg/day VPA (i.p.) injection were performed for 105 consecutive days after DMBA exposure; (B) HE staining for the morphology of tissues in the indicated groups; (C) Cleaved caspase-3 was analyzed in the indicated groups by IHC and Western blotting. Quantification of quantity of cleaved caspase-3 positive cells was shown. Data were derived from three independent experiments (mean ± SD). *P*-values were calculated by Student's *t*-test; (**$P < 0.01$; ns, not significant); (D) Representative images from immunofluorescence staining of vessels ($CD31^+$: green) were shown. Nuclei were counterstained with DAPI. Quantification of average fluorescent intensity was shown. Data were derived from three independent experiments (mean ± SD). *P*-values were calculated by Student's *t*-test (**$P < 0.01$; ns, not significant).

marker CD31, and found that the intervention of VPA (50 mg/kg or 100 mg/kg) reduced the vascular density, inhibited the growth of blood vessels, thus reducing the ability of tumor metastasis and invasion in DMBA-induced tumor (Fig. 1D, $P < 0.01$).

To investigate whether the observed VPA-regulated inhibition of tumor growth is associated with the immune response, we conducted the following experiments. Firstly, IHC staining of macrophage surface markers F4/80 and CD68 was conducted. We found that VPA promoted the infiltration of macrophages into the tumors (Fig. 2A and B). There was no difference observed between either F4/80 staining (Fig. 2A) or CD68 staining (Fig. 2B) after VPA (50 mg/kg or 100 mg/kg) treatments ($P > 0.05$). However, the number of positive macrophages was significantly increased in the DMBA groups after VPA intervention ($P < 0.05$), suggesting that the immune system is activated and that VPA promoted the infiltration of macrophages within the DMBA-induced breast tumors. Next, we explored the origin of these macrophages. Since CD11b is expressed in bone marrow line cells and is usually used as a marker of myeloid-derived differentiated cells (Rosetti and Mayadas, 2016; Solovjov et al., 2005), we performed IHC staining with CD11b. We found that $CD11b^+$ cells were significantly increased after VPA intervention in DMBA-induced tumors ($P < 0.05$) but not in normal breast tissues ($P > 0.05$, Fig. 2C), indicating that VPA might induce the increase of $CD11b^+$ cells in the tumors. Subsequently, we performed immunofluorescence co-localization staining with CD11b and F4/80, we found that the co-localization ratio of F480: CD11b increased after VPA intervention in DMBA-induced tumors ($P < 0.01$, Fig. 2D), supporting the proposition that VPA may promote the infiltration of myeloid-derived macrophages into the tumors.

3.2. VPA promotes the polarization of macrophages towards M1 phenotype in breast tumors and towards M2 phenotype in normal breast tissues

We next investigated whether VPA could affect the polarization of macrophages in DMBA-induced breast tumors and normal beast tissues. By RT-qPCR, we found that the surface marker CD86 of M1 macrophages was significantly increased while the surface marker CD163 of M2 macrophages was significantly decreased after VPA intervention in DMBA-induced breast tumors, respectively ($P < 0.01$). The increased ratio of CD86: CD163 after VPA intervention in DMBA-induced breast tumors ($P < 0.01$, Fig. 3A) suggests that VPA may promote the polarization of macrophages towards the M1 phenotype in DMBA-induced breast tumors. The ratio of iNOS (M1 macrophages functional marker) to Arg-1 (M2 macrophages functional marker) was also significantly increased after VPA (100 mg/kg) intervention of the DMBA-induced tumors ($P < 0.05$, Fig. 3B).

We also observed that the pro-inflammatory factors associated with the M1 phenotype, including IL-12, TNF-α and IFN-γ were all increased after the intervention of VPA ($P < 0.01$, Fig. 3C). However, the anti-inflammatory factors IL-10 and TGF-β related to M2 phenotype were

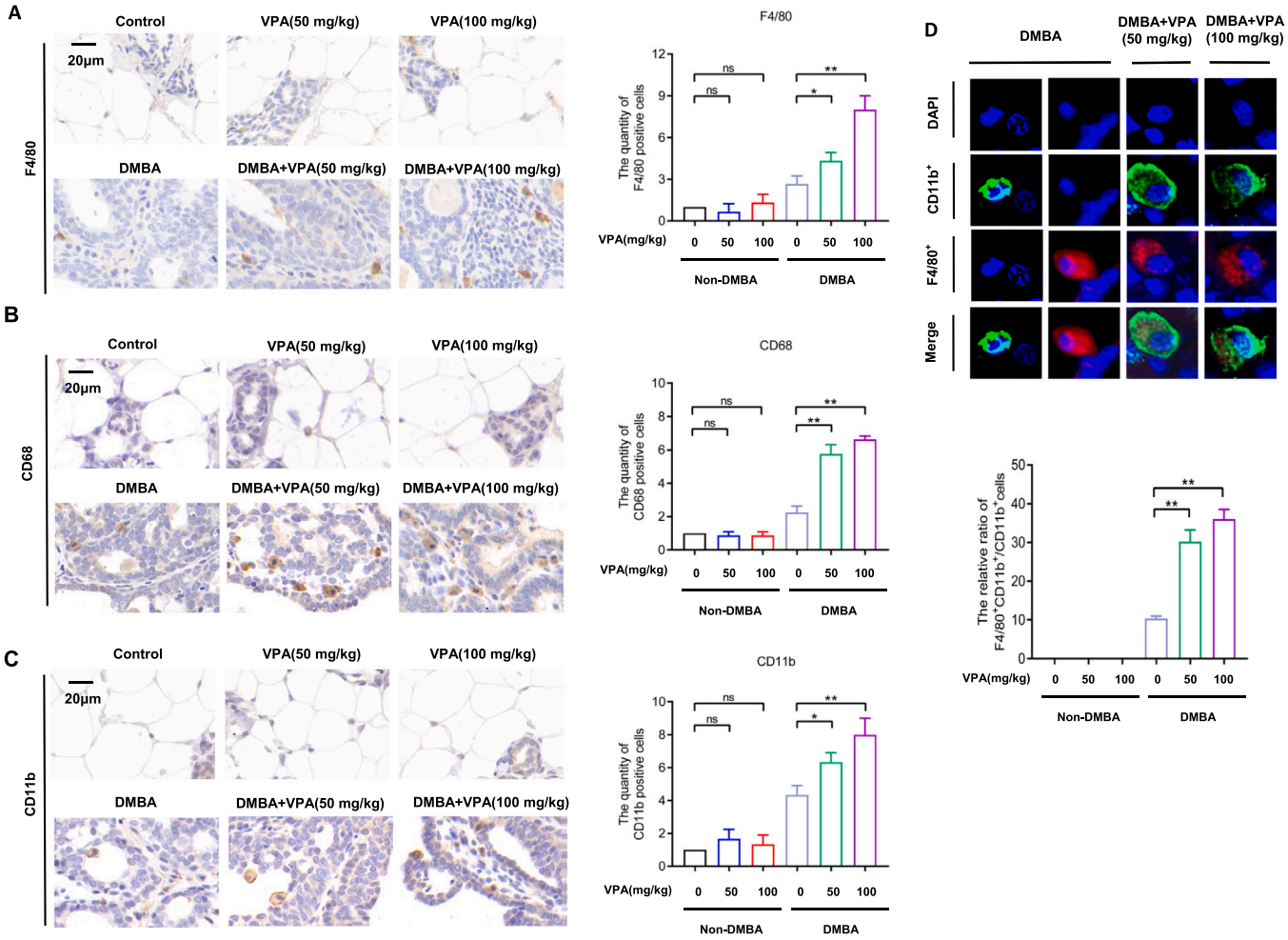

Fig. 2. VPA regulates infiltration of myeloid macrophages to enhance the intervention of breast tumors. (A&B) IHC was performed to stain the macrophages markers F4/80 (A), CD68 (B), and the myeloid marker CD11b (C) in the indicated groups; Data were derived from three independent experiments. Bars represent mean ± SD; $*P < 0.05$; $**P < 0.01$; ns, not significant. (D) Immunofluorescence co-staining of myeloid cells ($CD11b^+$: green) and macrophages ($F4/80^+$: red). Data were derived from three independent experiments. Bars represent mean ± SD; $**P < 0.01$; ns, not significant.

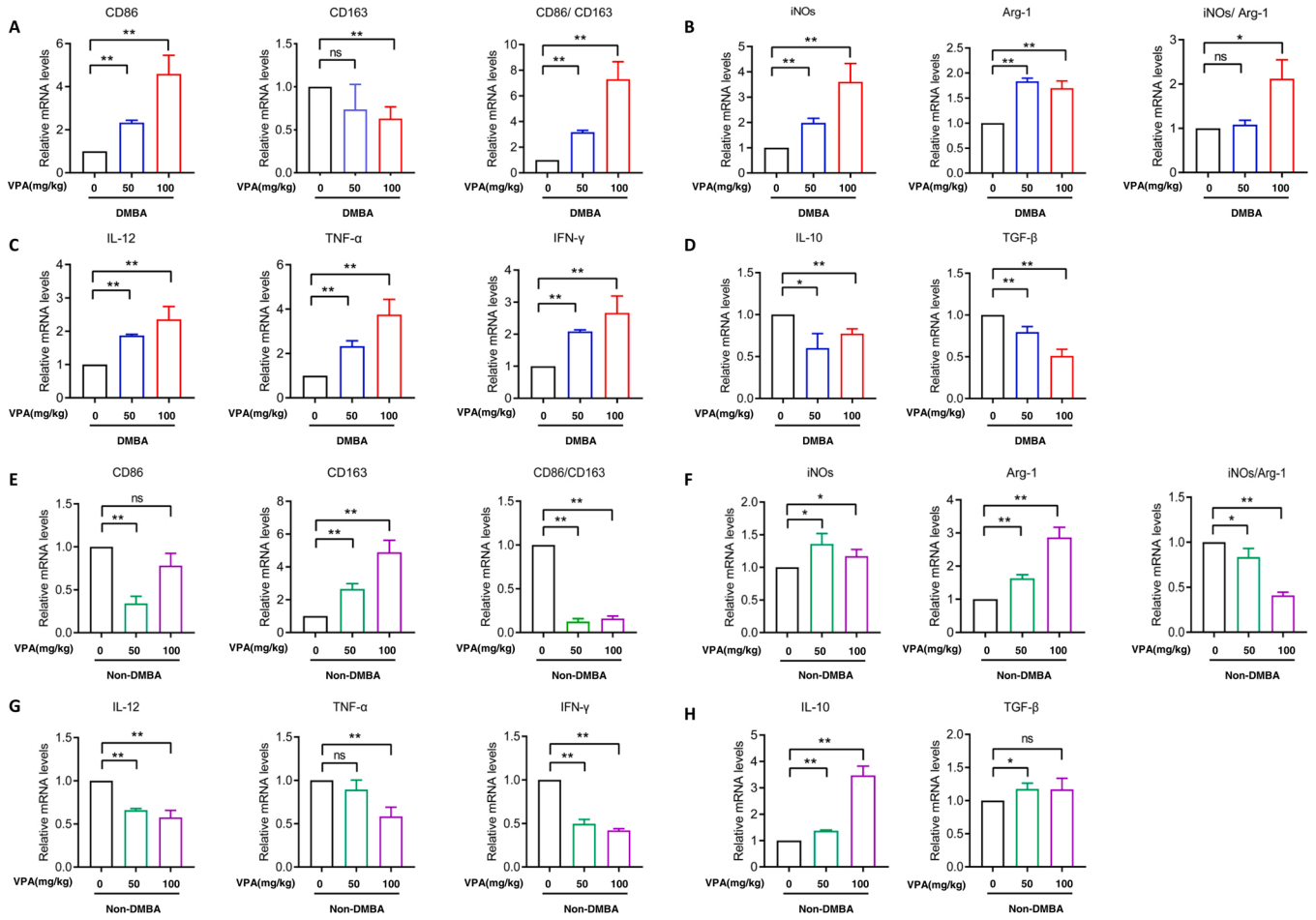

Fig. 3. VPA reprograms macrophages polarization in normal tissues and tumors. (A) The mRNA expression levels of CD86 (M1 macrophages surface marker) and CD163 (M2 macrophages surface marker) in DMBA-induced breast tumors were determined by RT-qPCR; Data were derived from three independent experiments. Bars represent mean ± SD; $^{**}P < 0.01$; ns, not significant. (B) The mRNA expression levels of iNOS (M1 macrophages functional marker) and Arg-1 (M2 macrophages functional marker) in DMBA-induced breast tumors were determined by RT-qPCR; Data were derived from three independent experiments. Bars represent mean ± SD; $^{*}P < 0.05$; $^{**}P < 0.01$; ns, not significant. (C&D) The mRNA expression levels of pro-inflammatory factor IL-12, TNF-α, IFN-γ (C) and anti-inflammatory factor IL-10, TGF-β (D) in DMBA-induced breast tumors were determined by RT-qPCR; Data were derived from three independent experiments. Bars represent mean ± SD; $^{*}P < 0.05$; $^{**}P < 0.01$. (E&F) The mRNA expression levels of CD86, CD163 (E) iNOs and Arg-1 (F) in breast tissues; Data were derived from three independent experiments. Bars represent mean ± SD; $^{*}P < 0.05$; $^{**}P < 0.01$. (G&H) M1 macrophages-related factors IL-12, TNF-α, IFN-γ (G) and M2 macrophages-related factors IL-10, TGF-β (H) in breast tissues were measured by RT-qPCR. Data were derived from three independent experiments. Bars indicate mean ± SD. *P*-values were calculated by Student's *t*-test; $^{*}P < 0.05$; $^{**}P < 0.01$; ns, not significant.

decreased after VPA intervention in DMBA-induced breast tumors ($P < 0.05$, Fig. 3D). These data indicated that VPA promoted the polarization of macrophages to the M1 phenotype and the secretion of pro-inflammatory factors in DMBA-induced breast tumors.

Conversely, the mRNA levels of the M1 macrophage surface marker CD86 was decreased and the M2 macrophage surface marker CD163 was significantly increased, respectively. The ratio of CD86: CD163 was decreased after VPA intervention in the normal breast tissues ($P < 0.01$, Fig. 3E) and the ratio of iNOS: Arg-1 was also significantly decreased after VPA intervention ($P < 0.05$, Fig. 3F). Meanwhile, M1 macrophages related inflammatory factors (IL-12, TNF-α and IFN-γ) were decreased ($P < 0.05$, Fig. 3G) and M2 macrophages related inflammatory factors (IL-10 and TGF-β) were elevated after VPA intervention in the normal breast tissues ($P < 0.05$, Fig. 3H), indicating that the macrophages polarized to the M2 phenotype and anti-inflammatory factors were secreted after VPA intervention in the normal breast tissues. Taken together, these data support the proposition that VPA promotes distinct polarization of macrophages in DMBA-induced breast tumors as compared to the normal breast tissues.

3.3. VPA activates macrophages with high phagocytosis and $CD8^+$ T lymphocytes in breast tumors

EpCAM is an early tumor-associated antigen, which is often used as a marker of tumor cells (Armstrong and Eck, 2003; Baeuerle and Gires, 2007). To test whether VPA regulates the phagocytosis of macrophages, we examined the co-localization of F4/80 and EpCAM. We found that the proportion of F4/80 and EPCAM co-location increased significantly after VPA intervention ($P < 0.01$, Fig. 4A), suggesting that the presence of tumor-derived apoptotic bodies in macrophages and VPA-induced macrophages exerts a higher phagocytosis ability.

We next performed IHC staining on $CD8^+$ T lymphocytes which mediate the anti-tumor immune response. We found that the number of $CD8^+$ T lymphocytes increased significantly after the intervention of VPA in DMBA-induced breast tumors ($P < 0.01$, Fig. 4B). Granzyme-B, a function marker of $CD8^+$ T lymphocytes, is the protease expressed by cytotoxic T lymphocytes (Trapani, 2001). Granzyme-B has the strongest apoptotic activity among all the enzymes, directly reducing downstream caspase substrates (Lord et al., 2003; Trapani and Sutton, 2003). We found that the number of positive Granzyme-B cells increased significantly after VPA intervention in DMBA-induced breast tumors

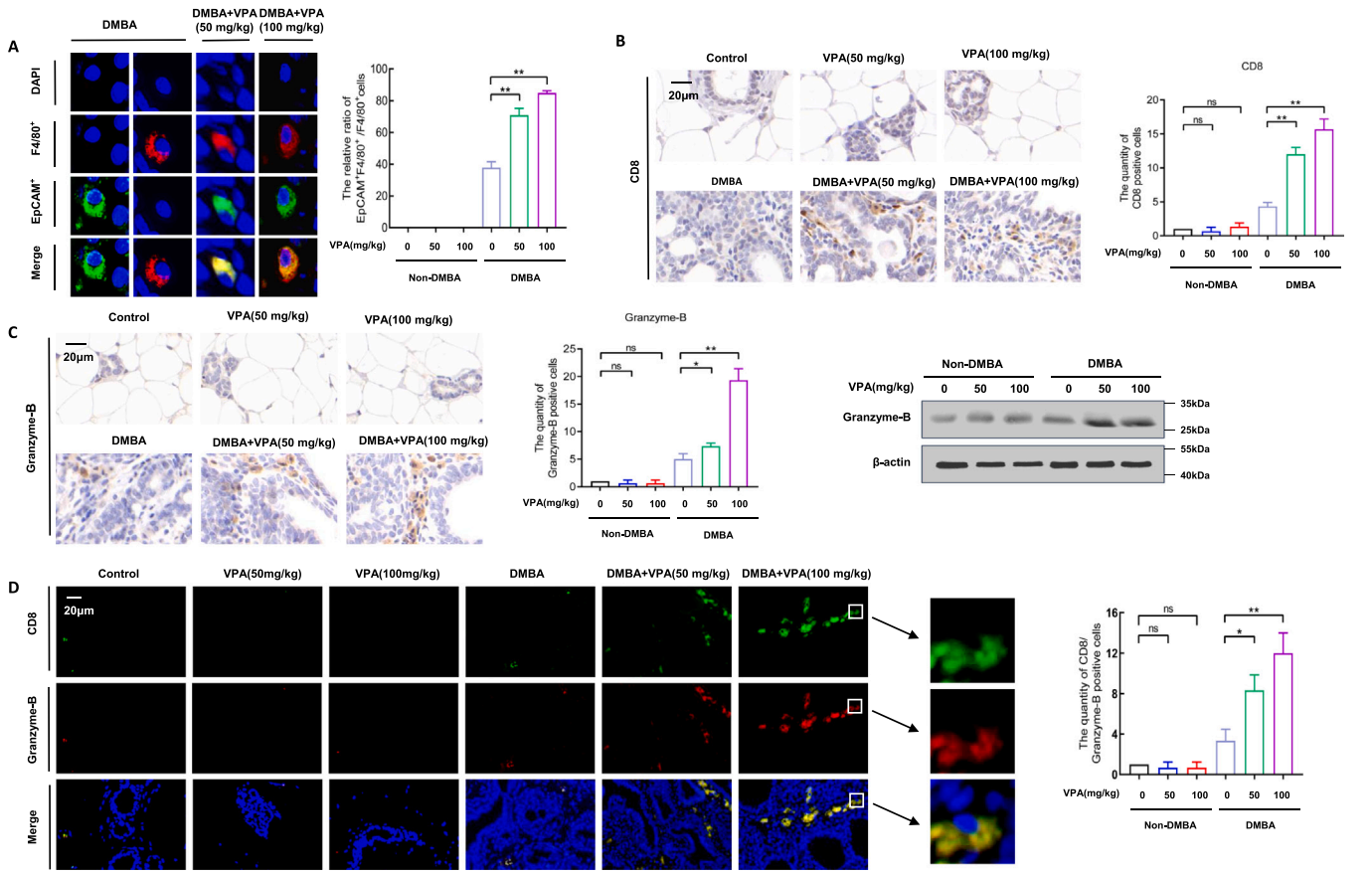

Fig. 4. VPA activates macrophages with high phagocytosis and CD8$^+$ T lymphocytes in breast tumors. (A) Immunofluorescence co-staining of macrophages (F4/80$^+$: red) and tumor-associated antigen (EpCAM$^+$: green); Data were derived from three independent experiments. Bars represent mean ± SD; $^{**}P < 0.01$. (B) CD8 analysis in the indicated groups by IHC staining; Data were derived from three independent experiments. Bars represent mean ± SD; $^{**}P < 0.01$; ns, not significant. (C) The expression of Granzyme-B was measured by IHC and Western blotting analysis. Data were derived from three independent experiments. Bars represent mean ± SD. *P*-values were calculated by Student's *t*-test. $^{*}P < 0.05$; $^{**}P < 0.01$; ns, not significant. (D) Immunofluorescence co-staining of CD8$^+$ T cells (green) and Granzyme$^+$ (red); Data were derived from three independent experiments. Bars represent mean ± SD; $^{*}P < 0.05$; $^{**}P < 0.01$.

($P < 0.05$) but not in the normal breast tissues by IHC staining ($P > 0.05$, Fig. 4C) and Western blotting ($P > 0.05$, Fig. 4C). We further performed immunofluorescence co-localization staining with CD8$^+$ and Granzyme-B and found that the co-localization ratio of CD8$^+$ and Granzyme-B increased after VPA intervention in DMBA-induced tumors ($P < 0.05$, Fig. 4D) but not in the normal breast tissues ($P > 0.05$, Fig. 4D). The data indicate that VPA activates CD8$^+$ T lymphocytes and promotes the secretion of Granzyme-B in DMBA-induced tumors. In summary, the effects of VPA intervention in breast tumors are in part associated with mediating the macrophage immune response.

3.4. *The protective effect of VPA on normal tissues may depend on macrophage-mediated immune response*

VPA intervention exerts protective effects on non-tumor tissues in our model. We next investigated whether macrophage-mediated immune response may be involved in the protective effect of VPA on normal tissues. Using BrdU staining, we observed no significant difference in BrdU staining of the normal spleen and small intestine tissues after VPA intervention ($P > 0.05$), but there was a decreased BrdU staining in the DMBA-induced spleen and small intestine ($P < 0.01$, Fig. 5A). Interestingly, VPA restored the proliferation ability of spleen and small intestine in the DMBA-induced tumors. However, we did not observe the same phenomenon in samples derived from liver and brain ($P > 0.05$, Fig. S1A).

We next performed IHC staining of CD68 in spleen and small intestine. We found that the positive number of CD68 is no significantly difference in the spleen and small intestine of normal tissues after VPA intervention ($P > 0.05$), but in the DMBA-induced tumors, the positive number of CD68 decreased significantly after the intervention of VPA ($P < 0.01$, Fig. 5B). The data suggest that the protective effect of VPA on normal tissues may be mediated by macrophages. However, we did not observe the same phenomenon in the liver, brain and lung ($P > 0.05$, Fig S1B). We further performed IHC staining on cleaved caspase-3 on the normal tissues and found no significant difference in the staining results of liver, brain, lung, spleen and small intestine after the intervention of VPA ($P > 0.05$, Fig. S2A).

We next investigated whether VPA could affect the polarization of macrophages on non-tumor tissues. We selected spleen and small intestine for the next series of experiment as previously noted, the macrophages were significantly decreased after the intervention of VPA. By RT-qPCR of the spleen, we found that the factors related to M1 phenotype, including CD86 and IFN-γ, were decreased the intervention of VPA ($P < 0.01$, Fig. 5C). The pro-inflammatory factors of TNF-α and IL-12 also showed a decreasing trend ($P > 0.05$, Fig. 5C).

The CD163, IL-10 and TGF-β related to the M2 phenotype tended to increase after VPA intervention, but there were no statistically significant differences ($P > 0.05$, Fig. 5C). By RT-qPCR analysis of the small intestine, we observed that the M1 phenotype pro-inflammatory factors, TNF-α and IFN-γ, decreased after the intervention of VPA ($P < 0.05$, Fig. 5D), but there was no statistically significant decreased on M1 macrophages surface marker CD86 and the pro-inflammatory factor IL-12 after the intervention of VPA ($P > 0.05$, Fig. 5D). Factors related to M2 phenotype, including CD163, IL-10 and TGF-β, were increased in the

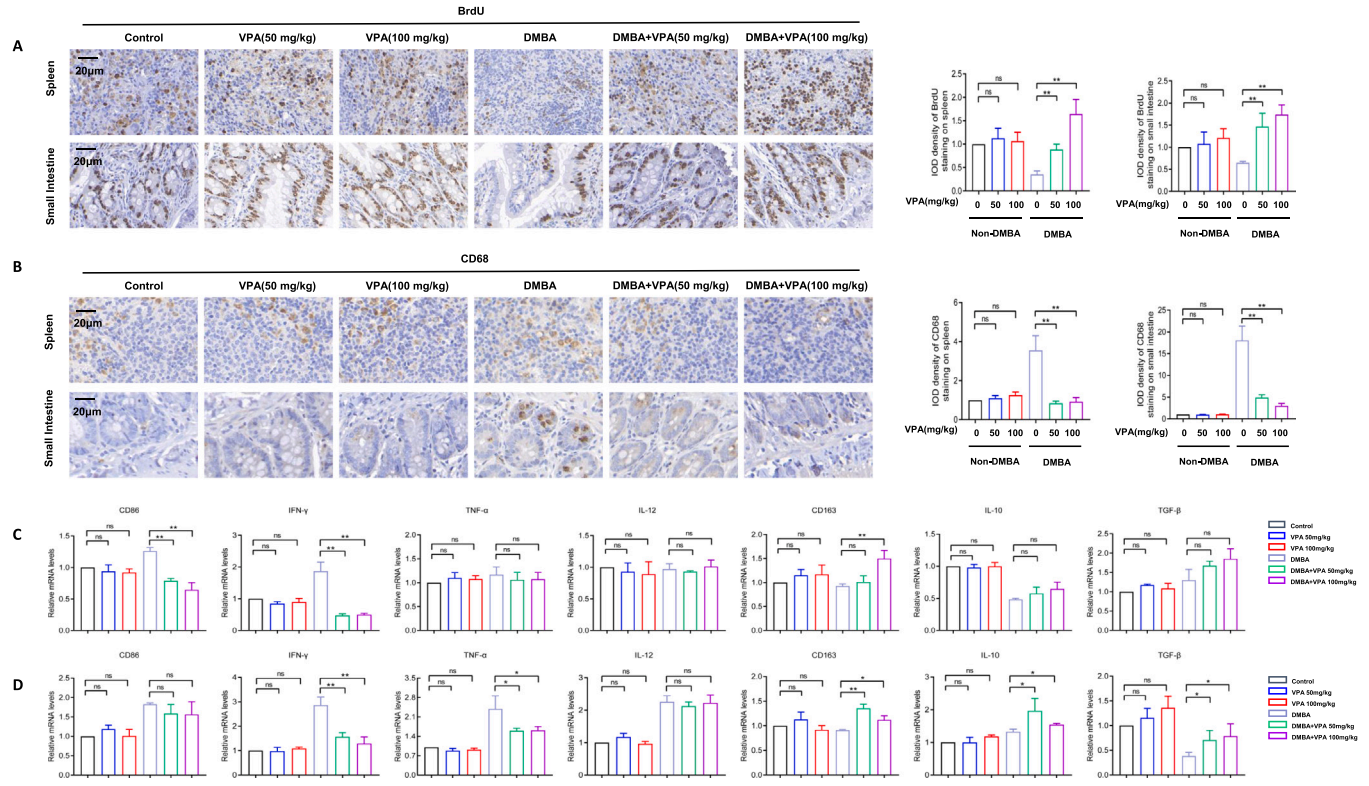

Fig. 5. VPA protects normal tissues by reducing infiltration of macrophages and reprograming macrophages polarization. (A&B) IHC staining of proliferation BrdU (A) and CD68 (B) in spleen and small intestine; Bars represent mean ± SD. *P*-values were calculated by Student's *t*-test. $^{**}P < 0.01$; ns, not significant. (C&D) RT-qPCR analysis of cytokines (CD86, IL-12, TNF-α, IFN-γ, CD163, IL-10, TGF-β) in spleen (C) and small intestine (D). Data in the graphs were derived from three independent experiments. Bars represent mean ± SD. *P*-values were calculated by Student's *t*-test. $^{*}P < 0.05$; $^{**}P < 0.01$; ns, not significant.

VPA-treated group ($P < 0.05$, Fig. 5D). These data suggest that macrophage-mediated immune response is involved in the observed VPA-mediated protective effects in normal tissues, that VPA promotes the polarization of macrophages to M2 phenotype and secrete some anti-inflammatory factors.

3.5. *The effect of VPA on the viability of vascular endothelial cells depends on the macrophages' polarization*

Through the *in vivo* experiments, we found that VPA reprograms macrophages to polarize towards the M1 phenotype and thus induces macrophages to secrete pro-inflammatory factors in the tumor microenvironment. By contrast VPA induces the polarization of macrophages towards the M2 phenotype and promote macrophages to secrete anti-inflammatory factors in the normal tissues microenvironment. We hypothesized that the effects of VPA-mediated anti-tumor and protection of normal tissues are dependent on the macrophages' polarization. Since we found the intervention of VPA reduced the vascular density and inhibited the growth of blood vessels in our animal experiments (Fig. 1D), we selected vascular endothelial cells (HUVEC) as an example to next investigate whether VPA-induced macrophages' polarization can affect the growth of vascular endothelial cells. For this experiment, we obtained the medium from MCF-10A normal cells or MCF10A-DMBA transformed cells as conditional medium to simulate the tissue microenvironment *in vivo*. First, the conditional medium of MCF-10A cells or MCF10A-DMBA cells were co-incubated with macrophages, RAW264.7 (Fig. 6A). After the RAW264.7 cells were incubated with MCF10A cells conditional medium and VPA for 24 h, we found that both surface markers, CD86 of M1 phenotype and CD163 of M2 phenotype increased ($P < 0.05$, Fig. 6B); however, the ratio of CD86: CD163 decreased and some M1 phenotype-associated pro-inflammatory factors such as IFN-γ, TNF-α and IL-12 were decreased after the intervention of VPA ($P < 0.05$, Fig. 6B). The M2 phenotype-associated factor, IL-10 ($P < 0.01$) displayed an increasing trend after the intervention of VPA (Fig. 6B). The data derived from RAW264.7 cells treated with MCF10A conditional medium and VPA for 48 h were also consistent with the observations at 24 h (Fig S3A). The RT-qPCR results indicate that VPA can induce macrophages to polarize to M2 phenotype in the conditional medium from normal cells.

When RAW264.7 cells were co-incubated with conditional medium of MCF10A-DMBA transformed cells and VPA for 24 h or 48 h, we found the mRNA levels of M1 macrophage surface marker, CD86 ($P < 0.01$), the ratio of CD86: CD163 ($P < 0.01$), as well as functional factors such as IFN-γ ($P < 0.01$), TNF-α ($P < 0.05$) and IL-12 ($P < 0.01$), were significantly increased (Fig. 6C, Fig. S3B). The surface marker of M2 macrophages, CD163 was significantly decreased ($P < 0.01$, Fig. 6C). The mRNA levels of anti-inflammatory factor IL-10 increased after 24 h VPA intervention ($P < 0.05$, Fig. 6C) but decreased significantly at 48 h ($P < 0.01$, Fig S3B), suggesting that VPA may promote the polarization of macrophages to M1 phenotype in the conditional medium from the incubation with tumor cells.

Additionally, we verified IL-12 and IL-10 by ELISA and the data were consistent with RT-qPCR analysis (Fig. 6D). When RAW264.7 cells were incubated with MCF10A cells conditional medium and VPA for 24 h, M1 phenotype-associated pro-inflammatory factors IL-12 was decreased and M2 phenotype-associated anti-inflammatory factors IL-10 was increased after the intervention of VPA, respectively ($P < 0.05$, Fig. 6D). By contrast, M1 phenotype-associated pro-inflammatory factors IL-12 was increased and M2 phenotype-associated anti-inflammatory factors IL-10 was decreased after the intervention of 0.4 mM VPA when RAW264.7 cells were incubated with MCF10A-DMBA cells conditional medium and VPA for 24 h ($P < 0.05$, Fig. 6D).

Next, the cell lysate from VPA-treated macrophages was incubated with vascular endothelial cells, HUVEC, to examine the cell viability at

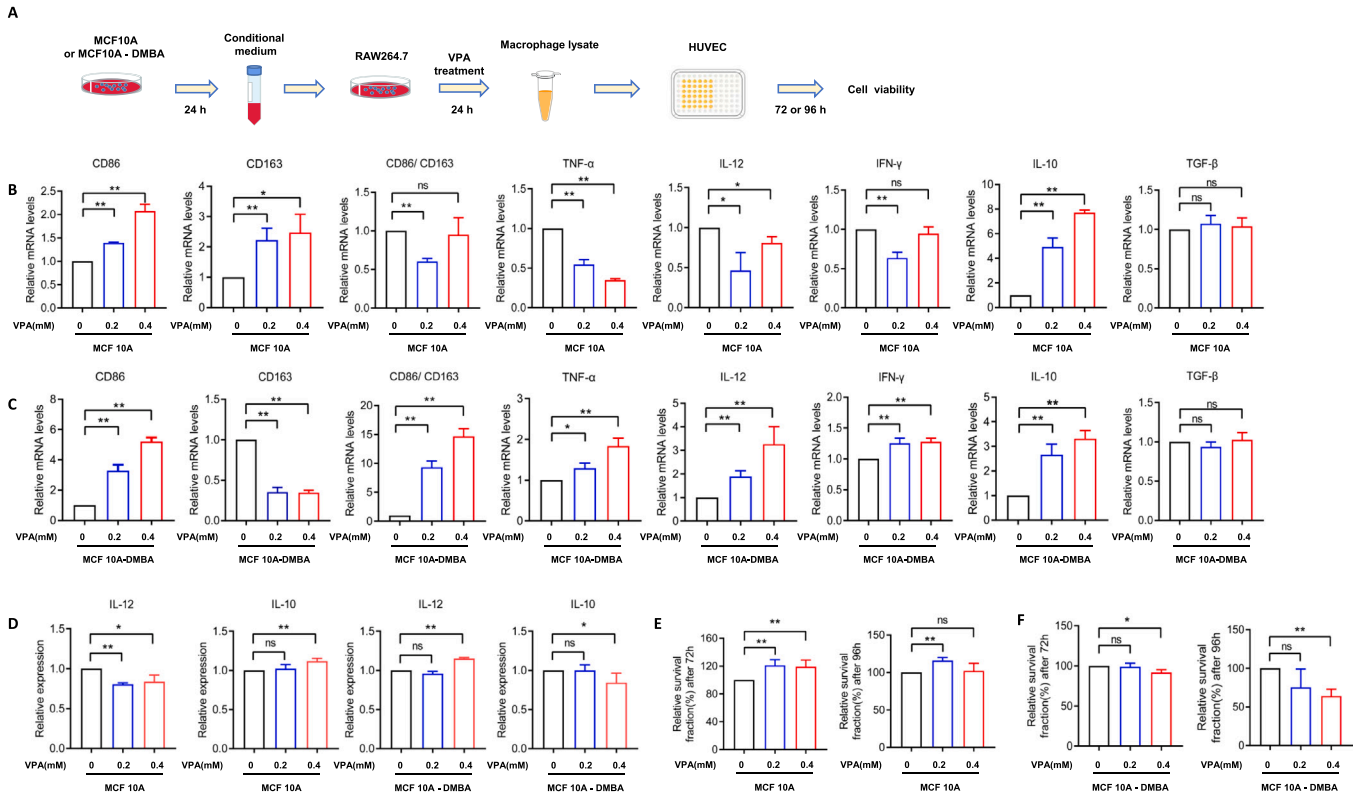

Fig. 6. The effect of VPA on the viability of vascular endothelial cells depends on the macrophages' polarization. (A) Workflow illustrates the analysis of MCF10A and MCF10A-DMBA conditional medium, macrophages polarization and the cell viability of HUVEC; (B&C) RT-qPCR analysis of cytokines (CD86, IL-12, TNF-α, IFN-γ, CD163, IL-10, TGF-β) of reprogrammed RAW264.7 macrophages under the treatment of MCF10A conditional medium (B) and MCF10A- DMBA conditional medium (C) after 24 h. Bars represent mean ± SD. *P*-values were calculated by Student's *t*-test. $*P < 0.05$; $**P < 0.01$; ns, not significant. (D) ELISA analysis of IL-12, IL-10 of reprogrammed RAW264.7 macrophages under the treatment of MCF10A conditional medium and MCF10A- DMBA conditional medium after 24 h. Bars represent mean ± SD. *P*-values were calculated by Student's *t*-test. $*P < 0.05$; $**P < 0.01$; ns, not significant. (E&F) HUVEC cells viability was detected by MTT at 72 h and 96 h, respectively: macrophages were incubated in conditional medium of MCF10A cells (E) and MCF10A- DMBA (F), and their lysate was incubated with HUVEC. Data in the graphs were derived from three independent experiments. Bars represent mean ± SD. *P*-values were calculated by Student's *t*-test. $**P < 0.01$; ns, not significant.

72 h and 96 h by MTT assay (Fig. 6A). We found that cell viability was increased in the VPA-treated macrophage lysate from the normal cell microenvironment ($P < 0.01$, Fig. 6F). In contrast, the cell viability of HUVEC tended to decrease after the incubation with VPA-treated macrophage's lysate in conditional medium of MCF10A-DMBA cells, the difference was statistically significant after the intervention of 0.4 mM VPA ($P < 0.05$, Fig. 6F). The absorbance of cells was measured at 532 nm, the results were consistent with that at 490 nm by MTT assay (Fig. S3C, S3D). Together, the above results indicate that the cell viability depends on the polarization of macrophages, the conclusion is consistent with the results from the previous *in vivo* experiment. In summary, in the tumor microenvironment, VPA polarizes macrophages to the M1 phenotype, promotes macrophages to secrete pro-inflammatory factors and thus exerts an inhibitory effect on the growth of tumor cell and vascular endothelial cells. Under the normal microenvironment, VPA induces the polarization of macrophages towards the M2 phenotype, facilitates macrophages secreting anti-inflammatory factors, and has a protective effect on the growth of normal cell and vascular endothelial cells.

4. Discussion

In this study, we found that VPA intervened DMBA-induced primary breast cancer of rat model through macrophages-mediated immune response and exerted protective effects on normal tissues (such as spleen and small intestine). In the tumor microenvironment, VPA reprogramed macrophages to the M1 phenotype polarization, recruited $CD8^+$T cells and inhibited the growth of blood vessels. While in the normal tissues, VPA induces the polarization of macrophages towards the M2 phenotype, reduces the inflammatory response and protects the normal organs from damage caused by DMBA both *in vivo* and *in vitro*. Collectively, our data advances the proposition that VPA intervenes the tumorigenic mechanism of PAHs through the regulation of macrophage-mediated immune responses.

4.1. The immune response in DMBA-induced cancer of rat intervention model

PAHs exist widely in the environment and have been identified as the main organic pollutants that affect human health. Due to the unique physical and chemical properties, PAHs are difficult to degrade and influence ecological environment (Sazykin et al., 2021). In daily life, direct or indirect exposure to such pollutants can cause damage to a variety of human organs, and long-term exposure can lead to irreversible fatal damage (Harmsen and Rietra, 2018) and birth defects, such as preterm birth (Singh et al., 2008), oral clefts (Langlois et al., 2013), neural tube defects (Ren et al., 2011), neurodevelopmental risk (Wang et al., 2014a) and asthma with related symptoms (Al-Daghri et al., 2013). According to the U.S. Environmental Protection Agency, seven PAH compounds have been classified as probable human carcinogens: Benz(a)anthracene, benzo(a)pyrene, benzo(b)fluoranthene, benzo(k) fluoranthene, chrysene, dibenz(ah)anthracene, and indeno(1,2,3-cd) pyrene. Carcinogenicity of PAHs has been found in some occupational exposure of workers, such as the workers breathing exhaust fumes

(Armstrong et al., 2004; Wei See et al., 2006) and those involved in mining, metal working, or oil refining (Ravindra et al., 2008). Workers whom were exposed to high levels of PAHs had a significantly increased risk of skin, lung and prostate cancer (Barul and Parent, 2021; Boffetta et al., 1997; Zhou et al., 2021).

DMBA is a representative compound of PAHs, and is commonly used to study tumorigenesis of PAHs. We were successful in establishing a working therapeutic model of DMBA-induced primary tumors in female Sprague Dawley (SD) rats (Cai et al., 2021; Wang et al., 2014b). In this study, we investigated the immune mechanism of VPA intervention in the PAH-induced tumor using this model. Since the concentration of 200 mg/kg is suggested as the higher therapeutic dose (Jin et al., 2021), we opted for the lower therapeutic doses of 50 mg/kg and 100 mg/kg in order to investigate the efficacy of VPA and test whether if this low-cost, efficacious therapeutic agent may indeed have the potential to advance to human clinical trial. We acknowledge that further pharmacokinetic studies may be warranted to investigate the optimal therapeutic dose for human trial.

4.2. VPA intervened DMBA-induced primary breast cancer through macrophages-mediated immune response

In the tumor microenvironment, TAMs are one of the most abundantly infiltrating leukocyte populations. TAMs drive immune escape, mediate immunosuppression and stimulate tumor metastasis (Coussens and Pollard, 2011; Pollard, 2009). The recurrence of tumor in patients is tightly related to immune escape (Li et al., 2018, 2019), thus highlighting that the importance of TAMs in oncological immunotherapy. In general, TAMs have strong plasticity and are generally considered to be M2-like (Obeid et al., 2013). TAMs-related factors such as Arg-1, TGF-β and IL-10 can directly reduce the toxicity of T cells to tumor cells (Rodriguez et al., 2003), and TAMs also correlate with abnormalities of tumor vascular system (Qian and Pollard, 2010). The M1 type-related factor IL-12 can activate $CD8^+$ T cells, release the production of perforin and granzyme, thereby stimulating the anti-tumor response (Harbeck et al., 2019; Kanemaru et al., 2017; Tugues et al., 2015). M1-related factors (TNF-α, IFN-γ) are associated with anti-angiogenesis. Studies have shown that IFN-γ can interfere with vascular integrity and affect tumor progression (Guerriero et al., 2017; He et al., 2017; Jayasingam et al., 2019; Kapellos and Iqbal, 2016). Therefore, reprogramming TAMs may play an important role in tumor immunotherapy.

Accumulating evidence alerts to the anti-tumor effect of HDACi. For example, HDACi have been shown to increase the anti-tumor efficacy of hormone therapy in ERα-positive breast cancer models (Alao et al., 2004; Hodges-Gallagher et al., 2007; Morel et al., 2020; Thomas et al., 2011). The HDACi have synergistic effects when used in combination with vascular endothelial growth factor inhibitors in exerting anti-angiogenic and anti-tumor effects in mouse models of various cancers (Ellis et al., 2009; Qian et al., 2004). The combination of VPA derivative and radiotherapy attenuated, and in some instances, ameliorated tumors growth through the activation of immune response in the tumor microenvironment (Cai et al., 2021). Recent studies on the immunity functions of HDACi and the histone acetylation (such as H3K9 or H3K27 acetylation) reported the observed anti-tumor effects may be closely related to the function of $CD8^+$ T cells (Henning et al., 2018). TMP195, an HDACi, is known to activate immune pathways to inhibit tumor development (Guerriero et al., 2017).

Our research revealed the immune effects of the VPA (an HDACi) in the process of tumor formation, indicating that VPA can inhibit tumor formation through anti-tumor immunity. During tumor formation, the apoptosis-related marker (cleaved caspase-3, Fig. 1C) was increased and the vascular endothelial marker (CD31, Fig. 1D) was significantly reduced in the tumor tissues after the intervention of VPA, and macrophages infiltration of the tumor tissue was noted (Fig. 2A, B). We hypothesized that the mechanism might involve the reprograming of TAMs. The macrophages typing test showed that M1-related pro-inflammatory factors (IL-12, IFN-γ, TNF-α) were increased in the intervention of VPA groups (Fig. 3C), angiogenesis was inhibited, the immune response was mediated by $CD8^+$ T cells (Fig. 4B, C). Meanwhile, M2-related factors (TGF-β, IL-10) that reduced $CD8^+$ T cell cytotoxicity were significantly reduced in the intervention of VPA groups (Fig. 3D). Therefore, the macrophage-involved immune response plays a pivotal role in the observed effects of VPA in attenuating tumorigenesis.

4.3. VPA exerted protective effects on normal tissues through macrophages-mediated immune response

Previous *in vivo* studies have shown that VPA can reduce the infiltration of macrophages in models of inflammation, indirectly indicating the bidirectional regulation of VPA. In the rat spinal cord injury model, VPA diminishes the infiltration of macrophages and provided neuroprotection (Lee et al., 2012). In the rat lung injury model, VPA reduces the expression of M1-related factors and polarizes macrophages toward M2-phenotype, which may be associated with the observed reduced inflammation and increased tissue repair (Venosa et al., 2017). In our research, we observed that VPA reduced macrophages-mediated inflammatory response in normal tissues (spleen and small intestine) (Fig. 5B), and promoted the polarization of macrophages to the anti-inflammatory M2 phenotype in our DMBA-induced models (Fig. 5C, D). The spleen is the largest lymphatic organ in the human body and the main place of specific immunity (Chadburn, 2000). As for the small intestine, there are lymphocytes, macrophages, eosinophils and other infiltrates in the lamina propria. We suspected that the above phenomenon may be very complicated and further studies are needed.

VPA reduced inflammation by decreasing the expression of M1-related factors, and also decreased the expression of iNOS and IL-12 under lipopolysaccharide and IFN-γ stimulation *in vitro* (Guo et al., 2007; Serrat et al., 2014). In addition, VPA can transform macrophages from pro-inflammatory M1 phenotype to anti-inflammatory M2 phenotype (Wu et al., 2012). In the cell model of our experiment, we co-cultured MCF10A cells with macrophages *in vitro* (Fig. 6A). We found that after the intervention of VPA, macrophages polarized to M2-phenotype and their related factors (CD163 and IL-10) increased (Fig. 6B).

In summary, our results revealed that VPA intervened DMBA-induced primary breast cancer in SD rats is protective of normal tissues (spleen and small intestine) and such mechanism of actions involve the macrophages-mediated immune response. Our study advances the support for further clinical exploration of HDACi in PAHs-induced tumors.

4.4. The anti-tumor immune mechanism activated by VPA needs further exploration and research

Although this study revealed that VPA plays a role in tumor chemoprevention by regulating the polarization state of macrophages, the following issues about the anti-tumor immune mechanism activated by VPA are worthy of further investigation. (1) The source of macrophages. Typically, mononuclear phagocytes originate from proliferating bone marrow precursor cells that differentiate into monocytes in the peripheral blood. Monocytes do not have the ability to proliferate in a stable state. During the infection stage, monocytes can migrate from peripheral blood into tissues and subsequently differentiate into dendritic cells and macrophages according to the surrounding inflammatory microenvironment (Auffray et al., 2009). Therefore, macrophages are generally considered to be differentiated from bone marrow hematopoietic stem cells. Under the action of chemokines in the tumor microenvironment, bone marrow-derived monocytes are recruited to tumor tissues and further differentiate into TAMs. Our study concluded that macrophages may originate from myeloid, but we could not rule out the possibility of other sources. The sources of macrophages are summarized into three types: myeloid development, the yolk sac, and local self-proliferation

(Ginhoux et al., 2010; Serbina et al., 2008). Therefore, the origin of VPA-promoted macrophages in tumor tissues requires further exploration. (2) Regulation of macrophage polarization. How does VPA affect macrophage polarization and promote the release of cytokines? And how does VPA exert a bidirectional regulatory effect on tumor tissue and normal tissue by regulating the polarization state of macrophages? Further clarification is also required. (3) The mechanism of the indirect tumor-killing effect of macrophages. In this study, it was found that VPA can promote the infiltration of macrophages and $CD8^+$ T cells in tumor tissues, whether macrophages exert antitumor effects by regulating $CD8^+$ T cells remains elusive. Studies have shown that IL-12 can activate $CD8^+$ T cells, release Granzyme-B and kill tumor cells (Harbeck et al., 2019; Kanemaru et al., 2017; Tugues et al., 2015). While M1 macrophages can secrete IL-12, suggesting that macrophages may also kill tumors through $CD8^+$ T cells indirectly to attain VPA-mediate prevention of tumorigenesis. (4) The role of histone deacetylation and the methylation status of DNA and histones: Since VPA as a potent HDACi may interfere with histone deacetylation and the methylation status of DNA and histone, it would be reasonable to explore whether histone modification is involved in the observed VPA's anti-tumor effect, such as whether VPA-mediated histone deacetylation (may including DNA and histone methylation) can affect the polarization of macrophages, also whether VPA-mediated histone deacetylation is involved in VPA-mediated protective effect in normal tissues (Gu et al., 2012; Mello, 2021; Milutinovic et al., 2007; Vidal and Mello, 2020).

In this study, we uncovered VPA regulates the polarization of macrophages to exert chemoprevention counteracting PAHs-induced the carcinogenic effects and further research is needed to illustrate the molecular mechanism.

Funding

This research was supported by grants from National Natural Science Foundation of China (No. 82173460), Natural Science Foundation of Shandong Province (ZR2020MH330), The Key Technology Research and Development Program of Shandong (2019GSF108083) and Cheeloo Young Scholar Project (21320082163154), Young Elite Scientists Sponsorship Program by CAST (2021QNRC001).

Authors contribution

Yisha Zhang, Zuchao Cai, David Lim, Chao Dong and Zhihui Feng designed the study, analyzed the data, and wrote the manuscript. Yisha Zhang performed most of the experiments. Zuchao Cai, Junxuan Peng, Beidi Jia and Guoliang Chu finished the rest part of the experiments in this study. Fengmei Zhang provided guidance for this work. All authors provided critical feedback on the manuscript. All authors read and approved the final manuscript.

Ethics approval and consent to participate

The studies of animal tissue were performed in accordance with the requirements of the Shandong University Human and Animal Ethics Research Committee (81472800, approved March 2014).

Declaration of Competing Interest

The authors declare that they have no known competing financial interests or personal relationships that could have appeared to influence the work reported in this paper.

Data Availability

The analyzed datasets generated during the current study are available from the corresponding author on reasonable request.

Acknowledgments

Not applicable.

Consent for publication

All authors consent to the publication of the manuscript.

Appendix A. Supporting information

Supplementary data associated with this article can be found in the online version at doi:10.1016/j.ecoenv.2022.113779.

References

Alao, J., et al., 2004. Histone deacetylase inhibitor trichostatin A represses estrogen receptor alpha-dependent transcription and promotes proteasomal degradation of cyclin D1 in human breast carcinoma cell lines. Clinical cancer research: an official journal of the American Association for. Cancer Res. 10, 8094–8104.
Al-Daghri, N.M., 2013. Polycyclic aromatic hydrocarbon exposure and pediatric asthma in children: a case-control study. Environ. Health 12.
Arlauckas, S., et al., 2017. In vivo imaging reveals a tumor-associated macrophage-mediated resistance pathway in anti-PD-1 therapy. Sci. Transl. Med. 9.
Armstrong, A., Eck, S.L., 2003. EpCAM - a new therapeutic target for an old cancer antigen. Cancer Biol. Ther. 2, 320–325.
Armstrong, B., et al., 2004. Lung cancer risk after exposure to polycyclic aromatic hydrocarbons: a review and meta-analysis. Environ. Health Perspect. 112, 970–978.
Auffray, C., et al., 2009. Blood monocytes: development, heterogeneity, and relationship with dendritic cells. Annu. Rev. Immunol. 27, 669–692.
Baeuerle, P.A., Gires, O., 2007. EpCAM (CD326) finding its role in cancer (vol 96, pg 417, 2007). Br. J. Cancer 96, 1491-1491.
Barul, C., Parent, M., 2021. Occupational exposure to polycyclic aromatic hydrocarbons and risk of prostate cancer. Environ. Health.: A Glob. Access Sci. Source 20, 71.
Bezza, F., Chirwa, E., 2016. Biosurfactant-enhanced bioremediation of aged polycyclic aromatic hydrocarbons (PAHs) in creosote contaminated soil. Chemosphere 144, 635–644.
Boffetta, P., et al., 1997. Cancer risk from occupational and environmental exposure to polycyclic aromatic hydrocarbons. Cancer Causes Control 8, 444–472.
Cai, Z., et al., 2021. Valproic acid-like compounds enhance and prolong the radiotherapy effect on breast cancer by activating and maintaining anti-tumor immune function. Front. Immunol. 12, 646384.
Chadburn, A., 2000. The spleen: anatomy and anatomical function. Semin. Hematol. 37, 13–21.
Coussens, L., Pollard, J., 2011. Leukocytes in mammary development and cancer. Cold Spring Harb. Perspect. Biol. 3.
DeNardo, D., et al., 2011. Leukocyte complexity predicts breast cancer survival and functionally regulates response to chemotherapy. Cancer Discov. 1, 54–67.
Ellis, L., et al., 2009. Targeting tumor angiogenesis with histone deacetylase inhibitors. Cancer Lett. 280, 145–153.
Epelman, S., et al., 2014. Origin and functions of tissue macrophages. Immunity 41, 21–35.
Ginhoux, F., et al., 2010. Fate mapping analysis reveals that adult microglia derive from primitive macrophages. Science 330, 841–845.
Gordon, S., Martinez, F., 2010. Alternative activation of macrophages: mechanism and functions. Immunity 32, 593–604.
Gu, S., et al., 2012. Valproic acid shows a potent antitumor effect with alteration of DNA methylation in neuroblastoma. Anti-Cancer Drugs 23, 1054–1066.
Guerriero, J., et al., 2017. Class IIa HDAC inhibition reduces breast tumours and metastases through anti-tumour macrophages. Nature 543, 428–432.
Guo, L., et al., 2007. Stat1 acetylation inhibits inducible nitric oxide synthase expression in interferon-gamma-treated RAW264.7 murine macrophages. Surgery 142, 156–162.
Harbeck, N., et al., 2019. Breast cancer. Nat. Rev. Dis. Prim. 5, 66.
Harmsen, J., Rietra, R., 2018. 25 years monitoring of PAHs and petroleum hydrocarbons biodegradation in soil. Chemosphere 207, 229–238.
He, W., et al., 2017. A Jak2-selective inhibitor potently reverses the immune suppression by modulating the tumor microenvironment for cancer immunotherapy. Biochem. Pharmacol. 145, 132–146.
Henning, A., et al., 2018. Epigenetic control of CD8 T cell differentiation. Nat. Rev. Immunol. 18, 340–356.
Hodges-Gallagher, L., et al., 2007. Inhibition of histone deacetylase enhances the anti-proliferative action of antiestrogens on breast cancer cells and blocks tamoxifen-induced proliferation of uterine cells. Breast Cancer Res. Treat. 105, 297–309.
Ino, Y., et al., 2013. Immune cell infiltration as an indicator of the immune microenvironment of pancreatic cancer. Br. J. Cancer 108, 914–923.
Jayasingam, S., et al., 2019. Evaluating the polarization of tumor-associated macrophages into M1 and M2 phenotypes in human cancer tissue: technicalities and challenges in routine clinical practice. Front. Oncol. 9, 1512.
Ji, M., et al., 2013. Valproic acid attenuates lipopolysaccharide-induced acute lung injury in mice. Inflammation 36, 1453–1459.

Jin, L., et al., 2021. Valproic acid triggers radiation-induced abscopal effect by modulating the unirradiated tumor immune microenvironment in a rat model of breast cancer. J. Radiat. Res.
Kanemaru, H., et al., 2017. Batf2Antitumor effect of through IL-12 p40 up-regulation in tumor-associated macrophages. Proc. Natl. Acad. Sci. USA 114, E7331–E7340.
Kapellos, T., Iqbal, A., 2016. Epigenetic control of macrophage polarisation and soluble mediator gene expression during inflammation. Mediat. Inflamm. 2016, 6591703.
Kim, B., et al., 2018. Panax notoginseng inhibits tumor growth through activating macrophage to M1 polarization. Am. J. Chin. Med. 46, 1369–1385.
Kim, K., et al., 2013. A review of airborne polycyclic aromatic hydrocarbons (PAHs) and their human health effects. Environ. Int. 60, 71–80.
Langlois, P., et al., 2013. Maternal occupational exposure to polycyclic aromatic hydrocarbons and risk of oral cleft-affected pregnancies. Cleft Palate-Craniofacial J.: Off. Publ. Am. Cleft Palate-Craniofacial Assoc. 50, 337-46.
Lee, J., et al., 2012. Valproic acid attenuates blood-spinal cord barrier disruption by inhibiting matrix metalloprotease-9 activity and improves functional recovery after spinal cord injury. J. Neurochem. 121, 818–829.
Li, X., et al., 2018. Lessons learned from the blockade of immune checkpoints in cancer immunotherapy. J. Hematol. Oncol. 11, 31.
Li, X., et al., 2019. Emerging predictors of the response to the blockade of immune checkpoints in cancer therapy. Cell. Mol. Immunol. 16, 28–39.
Li, X., et al., 2021. HDAC inhibition potentiates anti-tumor activity of macrophages and enhances anti-PD-L1-mediated tumor suppression. Oncogene 40, 1836–1850.
Liu, G., et al., 2021. The valproate mediates radio-bidirectional regulation through RFWD3-dependent ubiquitination on Rad51. Front. Oncol. 11, 646256.
Long, K., et al., 2019. Macrophages: Key orchestrators of a tumor microenvironment defined by therapeutic resistance. Mol. Immunol. 110, 3–12.
Lord, S., et al., 2003. Granzyme B: a natural born killer. Immunol. Rev. 193, 31–38.
Manjanatha, M., et al., 1996. Molecular analysis of lacI mutations in Rat2 cells exposed to 7,12-dimethylbenz[a]anthracene: evidence for DNA sequence and DNA strand biases for mutation. Mutat. Res. 372, 53–64.
Martinez, F., Gordon, S., 2014. The M1 and M2 paradigm of macrophage activation: time for reassessment. F1000prime Rep. 6, 13.
Medrek, C., et al., 2012. The presence of tumor associated macrophages in tumor stroma as a prognostic marker for breast cancer patients. BMC Cancer 12, 306.
Mello, M.L.S., 2021. Sodium valproate-induced chromatin remodeling. Front. Cell Dev. Biol. 9.
Milutinovic, S., et al., 2007. Valproate induces widespread epigenetic reprogramming which involves demethylation of specific genes. Carcinogenesis 28, 560–571.
Morel, D., et al., 2020. Combining epigenetic drugs with other therapies for solid tumours - past lessons and future promise. Nat. Rev. Clin. Oncol. 17, 91–107.
Morrison, C., 2016. Immuno-oncologists eye up macrophage targets. Nat. Rev. Drug Discov. 15, 373–374.
Obeid, E., et al., 2013. The role of tumor-associated macrophages in breast cancer progression (review). Int. J. Oncol. 43, 5–12.
Peng, J., et al., 2020. The intervention of valproic acid on the tumorigenesis induced by an environmental carcinogen of PAHs. Toxicol. Res. 9, 609–621.
Pollard, J., 2009. Trophic macrophages in development and disease. Nat. Rev. Immunol. 9, 259–270.
Qian, B., Pollard, J., 2010. Macrophage diversity enhances tumor progression and metastasis. Cell 141, 39–51.
Qian, D., et al., 2004. The histone deacetylase inhibitor NVP-LAQ824 inhibits angiogenesis and has a greater antitumor effect in combination with the vascular endothelial growth factor receptor tyrosine kinase inhibitor PTK787/ZK222584. Cancer Res. 64, 6626–6634.
Qiu, S., et al., 2018. Tumor-associated macrophages in breast cancer: innocent bystander or important player? Cancer Treat. Rev. 70, 178–189.
Ravindra, K., et al., 2008. Atmospheric polycyclic aromatic hydrocarbons: source attribution, emission factors and regulation. Atmos. Environ. 42, 2895–2921.
Reddy, J., et al., 2018. Mammary stem cell and macrophage markers are enriched in normal tissue adjacent to inflammatory breast cancer. Breast Cancer Res. Treat. 171, 283–293.
Ren, A., et al., 2011. Association of selected persistent organic pollutants in the placenta with the risk of neural tube defects. Proc. Natl. Acad. Sci. USA 108, 12770–12775.
Ring, A., et al., 2018. CBP/beta-Catenin/FOXM1 is a novel therapeutic target in triple negative breast cancer. Cancers 10.
Rodriguez, P.C., et al., 2003. L-arginine consumption by macrophages modulates the expression of CD3 xi chain in T lymphocytes. J. Immunol. 171, 1232–1239.
Roma-Rodrigues, C., et al., 2019. Targeting tumor microenvironment for cancer therapy. Int. J. Mol. Sci. 20.
Rosetti, F., Mayadas, T.N., 2016. The many faces of Mac-1 in autoimmune disease. Immunol. Rev. 269, 175–193.
Sazykin, I., et al., 2021. Polycyclic aromatic hydrocarbons, antibiotic resistance genes, toxicity in the exposed to anthropogenic pressure soils of the Southern Russia. Environ. Res. 194, 110715.
Serbina, N.V., et al., 2008. Monocyte-mediated defense against microbial pathogens. Annu. Rev. Immunol. 26, 421–452.
Serrat, N., et al., 2014. The response of secondary genes to lipopolysaccharides in macrophages depends on histone deacetylase and phosphorylation of C/EBPβ. J. Immunol. (Baltim., Md.: 1950) 192, 418–426.
Sharma, N., et al., 2013. The emerging role of histone deacetylase (HDAC) inhibitors in urological cancers. BJU Int. 111, 537–542.
Shi, B., et al., 2015. Distribution and source apportionment of polycyclic aromatic hydrocarbons in the surface soil of Baise, China. Environ. Monit. Assess. 187, 232.
Singh, V., et al., 2008. Comparison of polycyclic aromatic hydrocarbon levels in placental tissues of Indian women with full- and preterm deliveries. Int. J. Hyg. Environ. Health 211, 639–647.
Solovjov, D.A., et al., 2005. Distinct roles for the alpha and beta subunits in the functions of integrin alpha(M)beta. J. Biol. Chem. 280 (2), 1336–1345.
Song, R., et al., 2015. Valproic acid attenuates the expression of pro-inflammatory cytokines lipopolysaccharide-treated canine peripheral blood mononuclear cells (in vitro) and in a canine endotoxemia model (in vivo). Vet. Immunol. Immunopathol. 166, 132–137.
Su, B., et al., 2021. Valproic acid regulates HR and cell cycle through MUS81-pRPA2 pathway in response to hydroxyurea. Front. Oncol. 11, 681278.
Sun, K., et al., 2021. A review of human and animals exposure to polycyclic aromatic hydrocarbons: health risk and adverse effects, photo-induced toxicity and regulating effect of microplastics. Sci. Total Environ. 773, 145403.
Tang, X., 2013. Tumor-associated macrophages as potential diagnostic and prognostic biomarkers in breast cancer. Cancer Lett. 332, 3–10.
Tao, S., et al., 2020. The role of macrophages during breast cancer development and response to chemotherapy. Clin. Transl. Oncol. 22, 1938–1951.
Thomas, S., et al., 2011. Addition of a histone deacetylase inhibitor redirects tamoxifen-treated breast cancer cells into apoptosis, which is opposed by the induction of autophagy. Breast Cancer Res. Treat. 130, 437–447.
Trapani, J., 2001. Granzymes: a family of lymphocyte granule serine proteases. Genome Biol. 2, REVIEWS3 014.
Trapani, J.A., Sutton, V.R., 2003. Granzyme B: pro-apoptotic, antiviral and antitumor functions. Curr. Opin. Immunol. 15, 533–543.
Tugues, S., et al., 2015. New insights into IL-12-mediated tumor suppression. Cell Death Differ. 22, 237–246.
Venosa, A., et al., 2017. Regulation of nitrogen mustard-induced lung macrophage activation by valproic acid, a histone deacetylase inhibitor. Toxicol. Sci.: Off. J. Soc. Toxicol. 157, 222–234.
Vidal, B. d C., Mello, M.L.S., 2020. Sodium valproate (VPA) interactions with DNA and histones. Int. J. Biol. Macromol. 163, 219–231.
Wagner, J., et al., 2010. Histone deacetylase (HDAC) inhibitors in recent clinical trials for cancer therapy. Clin. Epigenetics 1, 117–136.
Wang, B.-L., et al., 2014a. Levels and neurodevelopmental effects of polycyclic aromatic hydrocarbons in settled house dust of urban dwellings on preschool-aged children in Nanjing. China Atmos. Pollut. Res. 5, 292–302.
Wang, F., et al., 2014b. Establishment of novel rat models for premalignant breast disease. Chin. Med. J. 127, 2147–2152.
Wang, S., et al., 2019. Regulation of Ca signaling for drug-resistant breast cancer therapy with mesoporous silica nanocapsule encapsulated doxorubicin/siRNA cocktail. ACS nano 13, 274–283.
Watanabe, S., et al., 2017. Valproic acid reduces hair loss and improves survival in patients receiving temozolomide-based radiation therapy for high-grade glioma. Eur. J. Clin. Pharmacol. 73, 357–363.
Wei See, S., et al., 2006. Health risk assessment of occupational exposure to particulate-phase polycyclic aromatic hydrocarbons associated with Chinese, Malay and Indian cooking. J. Environ. Monit.: JEM 8, 369–376.
Wu, C., et al., 2012. Histone deacetylase inhibition by sodium valproate regulates polarization of macrophage subsets. DNA Cell Biol. 31, 592–599.
Xu, J., Wang, Y.-h, 2011. Tumor-associated macrophages as promoters of tumor angiogenesis and metastasis. Fudan Xuebao (Yixueban) 38, 71–74.
Yang, X., et al., 2008. Identification of polycyclic aromatic hydrocarbons (PAHs) in soil by constant energy synchronous fluorescence detection. Spectrochim. Acta Part A Mol. Biomol. Spectrosc. 69, 400–406.
Zhang, H.-L., et al., 2012. Attenuated EAN in TNF-alpha deficient mice is associated with an altered balance of M1/M2 macrophages. PLoS One 7.
Zhou, S., et al., 2021. Associations of polycyclic aromatic hydrocarbons exposure and its interaction with XRCC1 genetic polymorphism with lung cancer: a case-control study. Environ. Pollut. 290, 118077.